Journal of Computational Physics 228 (2009) 7412–7425

Contents lists available at ScienceDirect

Journal of Computational Physics

journal homepage: www.elsevier.com/locate/jcp

# Modelling transient heat conduction in solids at multiple length and time scales: A coupled non-equilibrium molecular dynamics/continuum approach

Kenny Jolley, Simon P.A. Gill *

*Department of Engineering, University of Leicester, University Road, Leicester LE1 7RH, UK*

ARTICLE INFO

*Article history:*
Received 5 December 2007
Received in revised form 8 April 2009
Accepted 29 June 2009
Available online 3 July 2009

*Keywords:*
Molecular dynamics
Boundary conditions
Heat transfer
Multiscale modelling
Atomistic/continuum coupling

ABSTRACT

A method for controlling the thermal boundary conditions of non-equilibrium molecular dynamics simulations is presented. The method is simple to implement into a conventional molecular dynamics code and independent of the atomistic model employed. It works by regulating the temperature in a thermostatted boundary region by feedback control to achieve the desired temperature at the edge of an inner region where the true atomistic dynamics are retained. This is necessary to avoid intrinsic boundary effects in non-equilibrium molecular dynamics simulations. Three thermostats are investigated: the global deterministic Nosé–Hoover thermostat and two local stochastic thermostats, Langevin and stadium damping. The latter thermostat is introduced to avoid the adverse reflection of phonons that occurs at an abrupt interface. The method is then extended to allow atomistic/continuum models to be thermally coupled concurrently for the analysis of large steady state and transient heat conduction problems. The effectiveness of the algorithm is demonstrated for the example of heat flow down a three-dimensional atomistic rod of uniform cross-section subjected to a variety of boundary conditions.



## 1. Introduction

The boundary conditions for molecular dynamics (MD) simulations in the condensed phase are a compromise between correct representation of the far-field and minimization of the system size due to computational constraints. In recent years, concurrent multiscale methods have been developed for crystalline solids in which the complex response of the far-field is represented by a coarse-grained continuum region constructed from finite elements [1–13]. These multiscale modelling methodologies have mainly focussed on the far-field representation of the elastic field at zero or constant temperature, although a few authors have looked at the thermal far-field [9,10,13]. It is the aim of this paper to develop algorithms which firstly allow the temperature of an MD simulation to be precisely controlled away from thermal equilibrium, and secondly allow MD simulations to be concurrently coupled with a continuum representation of the thermal far-field.

The requirements of the continuum far-field depend on the nature of the simulation, generally either sampling or dynamics. If the purpose of simulation is sampling of near equilibrium or steady state quantities, then typically only slowly-changing thermodynamical or statistical quantities are of interest and inertial effects are small. Rapid changes occur in truly dynamic situations such as fast fracture. Finite temperature simulations are complicated by the reflection of high frequency phonons from the interface between the atomistic and continuum regions. This leads to energy trapping and localized heating [6]. Correct transmission of phonons across the interface [1,6,13] is only necessary if the far boundaries can be seen

* Corresponding author.
*E-mail address:* spg3@le.ac.uk (S.P.A. Gill).

0021-9991/$ - see front matter © 2009 Elsevier Inc. All rights reserved.
doi:10.1016/j.jcp.2009.06.035

during the simulation period (e.g. MEMS) or there are two atomistic regions which need to interact dynamically via the continuum medium (e.g. rapid growth of multiple cracks). We assume here that absorption of phonons at the interface is a sufficient requirement. This type of approach [10] has allowed the elastic boundary conditions to be specified at a position remote from the atomistic region. The majority of models are for isothermal problems, however. Constraining simulations to constant temperature can be highly restrictive, especially in cases where work is being done on the system and heat is being generated. Liu et al. [14] have recently demonstrated that MD simulations of nanoindentation are very sensitive to restricted thermostatic control. Keeping the boundary temperature constant also restricts simulations to be near to thermal equilibrium, whereas non-equilibrium conditions (e.g. temperature gradients) may be of interest. Elastically coupled atomistic/continuum simulations differ in their approach to (constant) finite temperature. Dupuy et al. [15] and Gill et al. [3] retain the dynamics of the atomistic system in the continuum region by allowing the finite element nodes to move under inertial forces. However, the dynamics of coarse-grained nodes are not physical and cannot model systems in which there is a temperature variation. This is because equipartition demands that a system will move towards a state in which each degree-of-freedom has the same thermal energy. If the number of degrees-of-freedom is reduced then the thermal energy it can store in the dynamics of those degrees-of-freedom is reduced. Therefore the kinetic energy per unit volume is not conserved through the body as the number of degrees-of-freedom per unit volume is not constant. Qu et al. [10] do not resolve the thermal vibrational motion of the atoms/nodes but link an isothermal molecular dynamics simulation to a quasi-static elasto-plastic continuum. As Qu et al. [10] consider an isothermal problem, the missing vibrational energy does not need to be represented in the continuum. A similar philosophy is adopted in this paper, except in the non-isothermal case the missing kinetic energy in the continuum does need to be explicitly conserved. This energy is represented by the usual continuum state variable, temperature, and is allowed to evolve according to the classical laws of heat conduction whilst interacting with the atomistic medium.

Three issues need to be addressed. Firstly, before any multiscale coupling can be considered, it is necessary to be able to precisely stipulate the boundary conditions of a non-equilibrium molecular dynamics (NEMD) simulation. This is investigated in the context of steady state heat conduction in Section 2. Secondly, for the coupled model, compatibility between the material parameters in the atomistic and continuum descriptions must be ensured. And thirdly, smooth transfer of information across the interface between the two models is required. These last two issues are discussed in Section 3.

## 2. Imposing a steady state temperature gradient on a molecular dynamics simulation

Most molecular dynamics simulations are sampled from the micro-canonical (constant energy) or canonical (constant temperature) ensembles. There have been a number of studies where a steady state temperature gradient has been imposed on an atomistic simulation [16–25]. The technique simply uses conventional thermostatting techniques to enforce different temperatures on opposite ends of the sample. These NEMD simulations can then be used to determine the effective thermal conductivity of the medium, $k$, from Fourier's law for macroscopic heat flow

$$q = -k\nabla T. \tag{2.1}$$

where $q$ is the heat flux (averaged over time and space) in the unthermostatted region between the thermostats, and $\nabla T$ is the "measured" steady state temperature gradient. However, as we shall see, the temperature gradient that develops between the thermostatted regions is not the temperature gradient that is expected from the stipulated end thermostat temperatures. The situation described above is therefore not as straightforward as it may appear. This is discussed further in this section where details of the atomistic simulation are given below, along with a discussion of potential difficulties.

### 2.1. Choosing a thermostat for NEMD simulation

In this paper we restrict our interest to ballistic heat transport in insulators via phonon interaction (i.e. conduction by electrons is neglected). This is an inherently non-linear phenomenon as phonons do not interact in the harmonic limit. The temporal evolution of a particle of mass $m_i$ at a position $\mathbf{x}_i$ in the main (unthermostatted) body of the system is described by the usual equations of motion

$$m_i\ddot{\mathbf{x}}_i = -\frac{\partial V_{TOT}}{\partial \mathbf{x}_i}. \tag{2.2}$$

where the potential energy of the system, $V_{TOT} = \sum_i \sum_{j>i} V(r_{ij})$, is the sum over all the interatomic potentials, $V(r_{ij})$, which are assumed here to be pairwise functions of the interatomic separation between atoms $i$ and $j$, $r_{ij} = |\mathbf{x}_i - \mathbf{x}_j|$. For the purposes of this paper we use the Lennard–Jones potential

$$V(r) = 4\varepsilon\left[\left(\frac{\sigma}{r}\right)^{12} - \left(\frac{\sigma}{r}\right)^{6}\right] \tag{2.3}$$

where only nearest neighbour interactions are considered. Physically, this potential is applicable to solid argon which has a melting temperature of roughly 80 K. In accordance with this we take $\varepsilon = 120k_B$, $\sigma = 3.4$Å and $m = 6.68\,\mathrm{e}\,10^{-26}$ kg [17,26,27] where $k_B$ is Boltzmann's constant. Note that the exact form of the interatomic potential is not important to the general

conclusions of this work. In fact, the primary philosophy behind the proposed modelling approach is to make it as simple and general as possible, so that it is not specific to particular details of the atomic model and can be implemented into a simulation code with only minor changes.

Consider a three-dimensional rod of Lennard–Jones atoms subjected to a temperature difference at each end. To establish a steady state temperature gradient along the rod, it is necessary to inject kinetic energy into one end of the rod and to remove it from the other end. This is achieved by the use of thermostatting algorithms. Two well-known examples of very different thermostats will be considered in this paper: the Langevin thermostat [6,20] and the Nosé–Hoover thermostat [20,28,29]. Like most thermostats, these have been designed to maintain a system at thermal equilibrium for constant temperature MD simulation. Their suitability for NEMD simulation is discussed further here.

The Langevin thermostat is a stochastic thermostat which adds a random force to the particle motion along with an appropriate damping term such that (2.2) becomes

$$m_i\ddot{\mathbf{x}}_i = -\frac{\partial V}{\partial \mathbf{x}_i} - \gamma m_i \dot{\mathbf{x}}_i + R\mathbf{f}, \tag{2.4}$$

where $\gamma$ is a damping coefficient, $-1 \leqslant R \leqslant 1$ is a uniformly distributed random variable and $f_n = \sqrt{\frac{6\gamma m_i T_c}{\Delta t}}$ is the magnitude of each component ($n = x, y$ or $z$) of the stochastic force $\mathbf{f}$ for a target temperature $T_c$ and a time step $\Delta t$. We describe the Langevin thermostat as a local thermostat as the target temperature is specified for each atom. This is advantageous for NEMD simulations as it allows for a spatially non-uniform temperature distribution to be specified at the boundaries. It is also very easy to implement in a simulation code. One drawback is that there is no feedback between the actual temperature and the target temperature for the Langevin thermostat. This is reasonable for equilibrium thermostatting, for which it was designed, but far from equilibrium there is no guarantee that the target temperature will be achieved or maintained.

The Nosé–Hoover thermostat is a deterministic thermostat which maintains the average temperature of an atomic ensemble at a target value. This is widely used for constant temperature dynamical simulations due to its symplectic, volume conserving, time-reversible Hamiltonian structure [3]. In this case the motion of a thermostatted particle is described by

$$m_i\ddot{\mathbf{x}}_i = -\frac{\partial V}{\partial \mathbf{x}_i} - \xi m_i \dot{\mathbf{x}}_i \quad Q\dot{\xi} = \frac{1}{M_T k_B T_c}\sum_{p=1}^{M_T} m_p \dot{\mathbf{x}}_p^2 - 1 \tag{2.5}$$

where $Q$ is a thermal mass, $\xi$ is a thermostatting variable and the summation is over all the thermostatted particles, $p = 1, \ldots, M_T$. This is a global thermostat in that it enforces an ensemble of particles to maintain an average kinetic energy over time. It preserves the average temperature but it does not have any control over the distribution of the temperature within the thermostatted region. Any temperature distribution which satisfies this average is possible. This is acceptable for isothermal simulations, in which there is no driving force for the distribution to be non-uniform. However, in NEMD simulations, where temperature gradients exist, the temperature distribution in the thermostatted region can be highly non-uniform. In this case, the temperature imposed at the edge of the thermostatted region will not be the target temperature. The Nosé–Hoover thermostat therefore also offers less potential for the stipulation of a spatial variation in temperature over a boundary, although Li and Weinan [5] have made some notable achievements in this regard by employing a number of Nosé–Hoover thermostats to control different regions of the simulation. One advantageous property, however, is that the temperature is controlled by feedback between the actual and target temperatures, so one can be confident that the desired average temperature has been achieved even in non-equilibrium simulations, unlike the Langevin thermostat. For rapidly changing transient boundary conditions, local thermostats are more responsive than global ones, which only react to a change in the global average temperature.

### 2.2. A standard NEMD simulation of a steady state temperature gradient

The steady state thermostatic control of a rectangular rod of 100 atoms in length with a periodic square cross-section of $8 \times 8$ atoms is investigated. The atoms are in the minimum energy hexagonal close packed structure and oriented such that an $8 \times 8$ cross-sectional slice represents a (100) plane. From a continuum perspective this is effectively a one-dimensional heat conduction problem, as there is expected to be no net heat flow or temperature variation within a cross-sectional slice of atoms. Therefore, each group of $8 \times 8$ atoms within a slice are referred to by an incremental index $j$. It is intended that the ends of the rod be maintained at different, uniform temperatures in order to achieve a prescribed steady state temperature gradient within some region of the simulation, $j = 0, \ldots, M$, where the true dynamics of the system are preserved. The thermostatted regions (TR) at the ends with the central true dynamics region (TDR) in the middle. This setup is illustrated in Fig. 1(a) for two TR of $M_T$ atomic slices. The separate regions are therefore defined by slice indices

$$j = \begin{cases} -M_T, \ldots, -1 & \text{for left TR} \\ 0, \ldots, M & \text{for TDR} \\ M+1, \ldots, M+M_T & \text{for right BR} \end{cases} \tag{2.6}$$

The Langevin damping coefficient, $\gamma = 1/2\omega_D$, is taken to be half the Debye frequency [10] (above which there are no modes). Solid argon has a Debye temperature of 93 K [30], which is equivalent to a Debye frequency of $\omega_D = 1.2 \times 10^{13}\,\mathrm{s}^{-1}$. The time

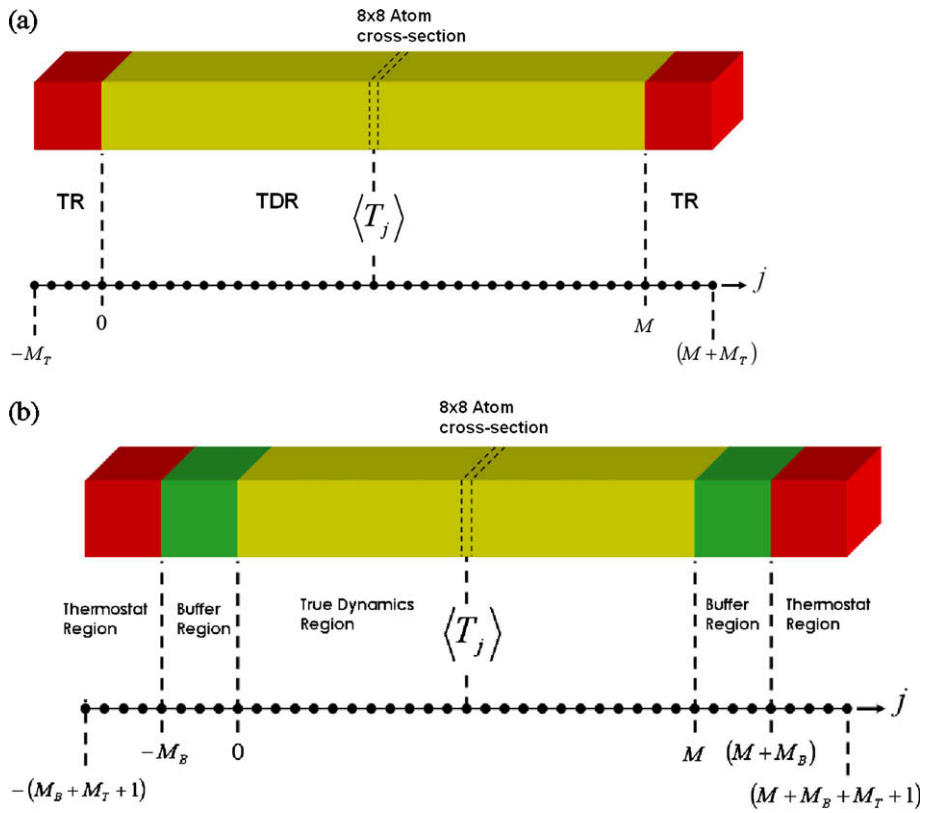


**Fig. 1.** Schematic of the three-dimensional molecular dynamics simulation. (a) The Lennard–Jones rod 100 atoms in length has an $8 \times 8$ square cross-section. Thermostats are used to regulate the temperature at the ends. The only net temperature gradient will be along the length of the rod. Therefore the time-ensemble averaged temperature in each cross-sectional slice of 64 atoms is expected to be uniform and is denoted $\langle T_j \rangle$ where $j$ is the index of the slice, shown in detail on the horizontal axis. A total of $M_T$ slices are thermostatted at each end (red TR region) in order to control the thermal boundary conditions of the inner true dynamics region of $M+1$ slices (yellow TDR region). (b) for accurate control of the thermal boundary conditions, a feedback algorithm is employed. In this case a buffer region of $M_B$ slices (green BR region) is introduced between the TRs and the TDR to avoid any corrupting boundary effects at the edge of the TRs. (For interpretation of the references to colour in this figure legend, the reader is referred to the web version of this article.)

step used in the integration of the equations of motion was chosen such that approximately 50 samples were performed in each oscillation, which equates to a time step of $\tau = 2.15 \times 10^{-14}$ s. Velocity Verlet time integration was used and micro-canonical simulations were performed to test energy conservation. The extremities of the rod are fixed ($\dot{x}_{-M_T} = \dot{x}_{M+M_T} = 0$) so that the atomic spacing is the zero Kelvin equilibrium spacing, although similar results are obtained for free end conditions.

The behaviour of three different thermostats is investigated: Nosé–Hoover (2.5), Langevin (2.4) and stadium damping. Stadium damping is a variant of Langevin which has been shown to be an effective means of phonon absorption [10,31] and importantly to produce the expected canonical ensemble [2]. In this case, the damping coefficient is a function of position, such that $\gamma = \gamma(\mathbf{x}_i)$. As shown in Fig. 2(c), it is linearly ramped from a maximum value of $\gamma = \gamma_0$ at the rod ends down to zero at the edge of the thermostatted region. This forms a diffuse interface which allows phonons to move into the damping region and be slowly absorbed as they move through it. This avoids many of the problems associated with phonon reflection at a sharp interface [13]. More sophisticated methods for sharp interfaces based on memory kernels have been considered in the literature [4,6–9] but these usually have to be calibrated for a particular potential, are derived from the harmonic approximation (for which heat conduction is not observed), and generally are not so readily implemented.

The thermostats are applied to a rod of 100 atoms in length with $M_T = 15$ slices of thermostatted atoms at each end and hence $M+1 = 70$ atomic slices in the TDR. The fixed target temperatures for the thermostats are $T_L$ and $T_R$ at the left ($L$) and right ($R$) ends, respectively. A temperature difference is imposed such that $T_R = 0.6T_L$. The effect of temperature is investigated by considering $T_L = 5$, 10, 25 and 50 K. Simulations are allowed to reach a steady state over a time of $10^6\tau$ and then the average temperature of the atoms in the $j$th slice, $\langle T_j \rangle = \left\langle 1/2 m_j \dot{x}_j^2 \right\rangle$, is determined over a subsequent period of $10^6\tau$, where $\langle \cdot \rangle$ denotes the time-ensemble average over the whole slice. The resulting steady state temperature distributions along the length of the rod are shown for the three thermostats in Fig. 2(a)–(c). From (2.1) it is expected that the temperature profile will vary linearly between the target temperatures at each end for a constant thermal conductivity (as illustrated by the dashed lines in Fig. 2). As found in previous works [16–25], the simulation results do not conform to this expectation.

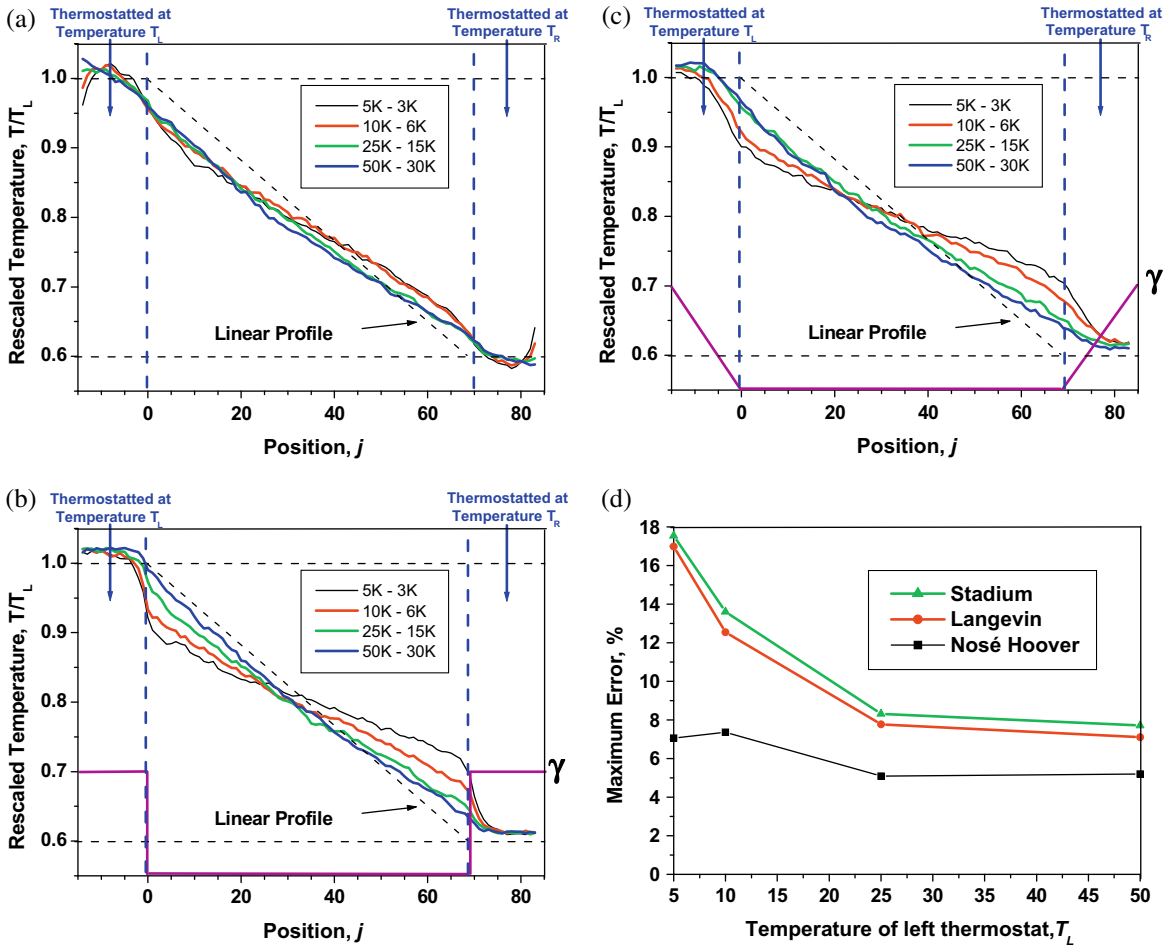


**Fig. 2.** Steady state temperature profile along the $8 \times 8 \times 100$ atomic rod shown in Fig. 1(a). The temperature difference is imposed by thermostatting the two end atoms such that the left hand thermostat temperature is $T_L = 5$, 10, 25 and 50 K and that at the right hand end is $T_R = 0.6T_L$. Results are shown for (a) a deterministic Nosé–Hoover thermostat, (b) a stochastic Langevin thermostat and (c) a variant of the Langevin thermostat, stadium damping. The expected steady state temperature distribution for a constant thermal conductivity is shown as a dashed line. The deviations from the expected result arise from end effects. (d) The maximum percentage error for each simulation shows that the error decreases as the temperature increases and is smallest for the Nosé–Hoover thermostat, although it is still greater than 5%.

There is a drop in the temperature at the edge of the thermostatted regions, such that the temperature gradient observed in the simulation is not the temperature gradient expected from the imposed temperature difference. The maximum deviation from the correct temperature profile (to be determined and shown in Fig. 3) is plotted in Fig. 2(d). The percentage error is quite significant and clearly observable in all the temperature profiles, ranging from 5 to 20%. The largest errors are seen at low temperatures (where phonon interactions, due to sampling non-linearities in the potential, are reduced) and for stochastic thermostats (Langevin and stadium). This effect has been widely observed and is generally attributed to phonon mismatch at the interface between the thermostatted and unthermostatted regions [22]. The effect can be even more pronounced for other potentials, e.g. silicon [22]. For real physical interfaces this is known as the Kapitza effect, where it is observed that the thermal conductivity, like most physical properties, deviates from the bulk value near an interface. Even if the interface is artificial, as is the case here, it is difficult to avoid. To understand the origin of this boundary effect, and why its magnitude depends on the thermostatting method, we refer to the Green–Kubo formula [22]. This linear response theory allows the thermal conductivity to be determined from equilibrium simulations, and is often used for this purpose rather than NEMD simulations. It states that the conductivity is proportional to the long-time average of the heat flux autocorrelation. Assuming local equilibrium, the conductivity between slices $j$ and $j+1$ is proportional to

$$k_j \propto \lim_{t\to\infty} \int_0^t \langle q_j(s) q_j(0) \rangle ds \tag{2.7}$$

where $q_j(t)$ is the instantaneous net heat flux between slices $j$ and $j+1$. The net energy flux between particles is therefore due to long-term correlations between their motions. Any thermostat will always necessarily alter a particles motion and corrupt

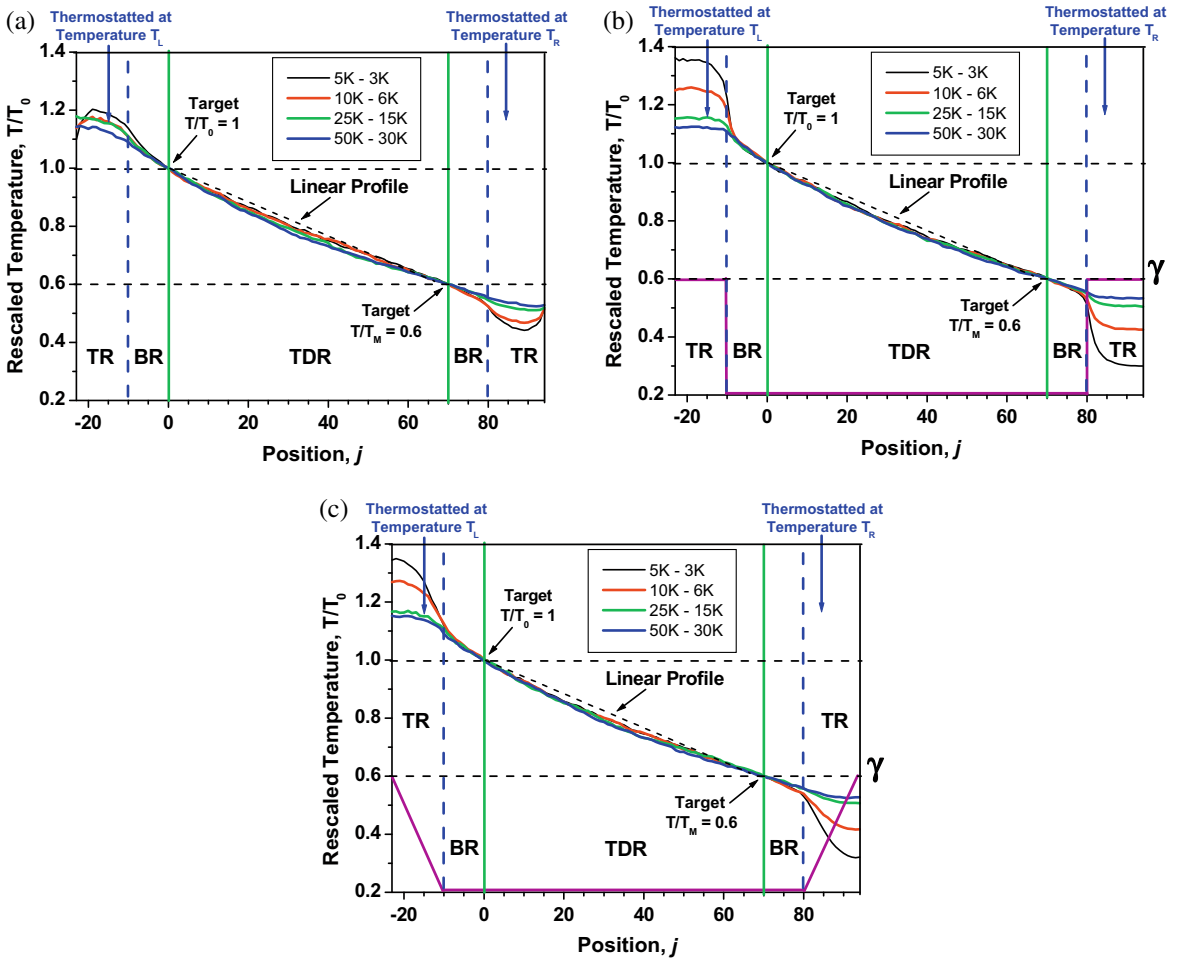


**Fig. 3.** Precise imposition of a steady state temperature gradient along a three-dimensional ($8 \times 8 \times 100$ atom rod) NEMD simulation by feedback control of the thermal boundary conditions using (2.9) for (a) Nosé–Hoover, (b) Langevin, and (c) stadium damping thermostats. The time-averaged temperature profile along the rod is shown. The temperatures in the left and right thermostatted regions ($M_T = 15$ atomic slices = 960 atoms each) are regulated at $T_L$ and $T_R$ by (2.9) such that the prescribed target temperatures in atomic slices $j = 0$ and $j = 69$, respectively are maintained at $T_0 = 5$, 10, 25 and 50 K and $T_M = 0.6T_0$ for all four cases. A buffer region (BR) of $M_B = 10$ atomic slices is introduced between the thermostatted regions (TR) and the true dynamics region (TDR) to avoid Kapitza and other effects at the TR/BR interfaces. Note that the temperature variation within the TR is non-uniform and unpredictable. The stochastic Langevin and stadium damping thermostat require a much larger temperature difference between the TR at either end to impose the same temperature gradient than the deterministic Nosé–Hoover thermostat. The Kapitza effect at the boundaries is smallest for the stadium damping case. The profiles in the TDR are not exactly linear due to changes in the thermal conductivity with temperature.

this correlation and hence reduce the thermal conductivity at the edge of the thermostatted region. The Nosé–Hoover thermostat in Fig. 2(a) is seen to be better than the Langevin and stadium thermostats in Fig. 2(b) and (c) as deterministic methods naturally exhibit longer correlation times than (uncorrelated) stochastic methods. In the steady state, the time-averaged heat flux at each point must be constant for conservation of energy. In this case (2.1) shows that the effective conductivity at a point must be proportional to the inverse of the temperature gradient such that $k \propto 1/\nabla T$. There is a larger-than-expected temperature gradient at each end for the Langevin and stadium thermostats in Fig. 2(b) and (c). This implies that the conductivity is small at the thermostat interfaces and that these stochastic thermostats strongly affect any temporal correlations between particle motions at that point. The case for the Nosé–Hoover thermostat in Fig. 2(a) is improved, although the boundary conductivity is still reduced. An elementary solution to these adverse, non-linear boundary effects is proposed in the next sub-section.

### 2.3. Improved boundary conditions with feedback control for steady state NEMD simulation

The steady state thermostatic control of a rectangular rod is again investigated, but to avoid the problems due to boundary effects and global thermostatting methods, the thermostatted regions (TR) at the ends are separated from the central true dynamics region (TDR) in the middle by two small buffer regions (BR). This setup is illustrated in Fig. 1(b) for two BR of $M_B$ atomic slices and two TR of $M_T$ slices. The separate regions are therefore defined by slice indices

$$j = \begin{cases} -(M_B + M_T), \ldots, -(M_B + 1) & \text{for left TR} \\ -M_B, \ldots, -1 & \text{for left BR} \\ 0, \ldots, M & \text{for TDR} \\ M+1, \ldots, M+M_B & \text{for right BR} \\ M+M_B+1, \ldots, M+M_B+M_T & \text{for right TR} \end{cases} \tag{2.8}$$

It has been previously noted that there is not a straightforward relationship between the temperature that is imposed on the TRs and the temperature gradient which develops between them in the TDR. To ensure that there is precise control of the temperature within the TDR, the average temperature of the atomic slices at the edges of this region, $\langle T_0 \rangle$ and $\langle T_M \rangle$ are determined, where $\langle T_j \rangle$ is the time-ensemble average of the temperature over all the atoms in slice $j$, as before. It is desired that these two atomistic temperatures attain the constant values $T_0$ and $T_M$, respectively in the steady state. The target temperatures in the left and right TRs, $T_L$ and $T_R$, must evolve to ensure that the actual temperatures at the periphery of the TDR ($\langle T_0 \rangle$ and $\langle T_M \rangle$) are maintained at the prescribed values ($T_0$ and $T_M$). A simple feedback loop is used to achieve this such that

$$\dot{T}_L = \frac{[T_0 - \langle T_0 \rangle]}{Q_T}, \quad \dot{T}_R = \frac{[T_M - \langle T_M \rangle]}{Q_T} \tag{2.9}$$

where the constant $Q_T$ determines the responsiveness of the thermostat. One benefit of this algorithm is that it provides feedback for the stochastic methods which was previously missing. Hence one can be certain that Langevin and stadium damping achieve the desired temperature.

Results are obtained for the same conditions as in Fig. 2, with $T_0$ = 5, 10, 25 and 50 K and $T_M = 0.6T_0$ with $M_T = 15, M_B = 10$ and a TDR of $M + 1 = 70$. These temperature profiles are shown in Fig. 3 for the three different thermostats under investigation, with $Q_T = 100\tau$ and a thermal mass of $Q = 10\varepsilon\tau$ for the Nosé–Hoover thermostat. It is found that all the thermostats correctly impose the prescribed temperatures at the boundaries of the TDR and that they all achieve a steady state in a similar time. Inspection of the temperature variation over time at every slice within the TDR shows that it reproduces the Boltzmann distribution (that one would expect at the equivalent equilibrium temperature). The temperature profiles are not exactly linear. This is because the thermal conductivity changes with temperature. The temperature profile is therefore most non-linear for the cases where the temperature range is greatest. The three principal differences between the three algorithms are in the TRs and the BRs. Firstly, the temperature distribution in the TRs is quite non-uniform for the Nosé–Hoover and Langevin thermostats. This is because there is an abrupt change in the dynamics of the particles between the TRs and BRs and, in the case of the global Nosé–Hoover thermostat, this is controlling the average temperature not the temperature distribution. The temperature distribution in the stadium damping case is more linear, which is in accordance with the linear variation in the damping parameter, $\gamma(x)$. Secondly, a major difference between the stochastic thermostats and the deterministic Nosé–Hoover thermostat in Fig. 3 is that a much greater difference between the thermostat target temperatures, $T_L - T_R$, is required for the stochastic thermostats to achieve the prescribed temperature difference, $T_0 - T_M$. This is expected from Fig. 2, where the stochastic Langevin thermostat is observed to corrupt the particle dynamics considerably leading to a larger drop in the conductivity at the interface with the thermostat region. This large temperature difference could be problematic if the lower target temperature in the thermostat region dropped below zero or the higher target temperature exceeded the melting point. However, this is only expected to be truly problematic in the presence of very high temperature gradients. The temperature gradient considered in this study is high for investigative purposes, but it is not unrealistic and can be easily attained when two surfaces at slightly different temperatures first come into contact for instance. The third difference between the thermostats is in the BRs. For the Nosé–Hoover thermostat the desired temperature gradient is only established within 5–6 atoms of the TR. For the Langevin thermostat there is a large drop in temperature over the first 2–3 atoms in the BR but then the correct temperature gradient is achieved. The best case is for the stadium damping thermostat, for which the boundary effect is small, and there is a smooth transition from the TR to the desired temperature gradient over 2–3 atoms. Hence it seems possible that the BR could be reduced in size for the stochastic algorithms. Note that energy is being injected by the thermostat into the left hand TR and removed from the right hand TR. Both ends are controlled by an identical algorithm which can handle either situation without modification. This is important when considering transient problems where the direction of heat flow across a boundary can reverse during the course of the simulation. The stadium damping algorithm produces the smoothest temperature profile across the TR and BR, is easy to implement, addresses each atom locally and provides a diffuse interface for phonon absorption. This method is therefore considered to be the best candidate for further implementation and is therefore the only thermostat considered in the final sections of this paper.

## 3. A coupled atomistic/continuum model for heat flow

The aim of this section is to demonstrate that a continuum representation of the NEMD simulation in Section 2 can be developed and concurrently coupled to an atomistic NEMD simulation to provide full control of the remote boundary conditions. A continuum model of the one-dimensional heat conduction problem is derived in Section 3.1. In this case the finite difference method is used. The model is initially developed in Section 3.2 within the context of the steady state analysis of the previous section. This is then extended to the fully transient case in Section 3.3, where the boundary conditions to the TDR are a function of time.

### 3.1. The continuum heat conduction model

A continuum finite difference model is employed in regions which overlap the TRs and the BRs, as shown in Fig. 4(a). The one-dimensional finite difference grid matches the initial regular positions of the atomistic slices in these regions. However, this is not a requirement of the model, for which the grid-spacing can be irregular and extend to any remote position. The nodal temperatures on the finite difference grid are denoted as $\tilde{T}_j$ and are at a fixed position $\tilde{x}_j$, where $j$ denotes the slice number. These temperatures can evolve by the usual finite difference algorithm

$$c\dot{\tilde{T}}_j = \tilde{q}_j - \tilde{q}_{j-1} \tag{3.1}$$

where

$$\tilde{q}_j = k\left(\frac{\tilde{T}_j + \tilde{T}_{j+1}}{2}\right)\frac{(\tilde{T}_{j+1} - \tilde{T}_j)}{(\tilde{x}_{j+1} - \tilde{x}_j)} \tag{3.2}$$

is the continuum heat flux between nodal points $j$ and $j+1$. The thermal conductivity $k(T)$ is assumed to be a function of temperature $T$. The constant $c$ is the heat capacity of an atom and is defined to be the amount of energy required to raise the temperature of an atom by 1 K. In the simple case of a classical three-dimensional crystal with pairwise interactions this

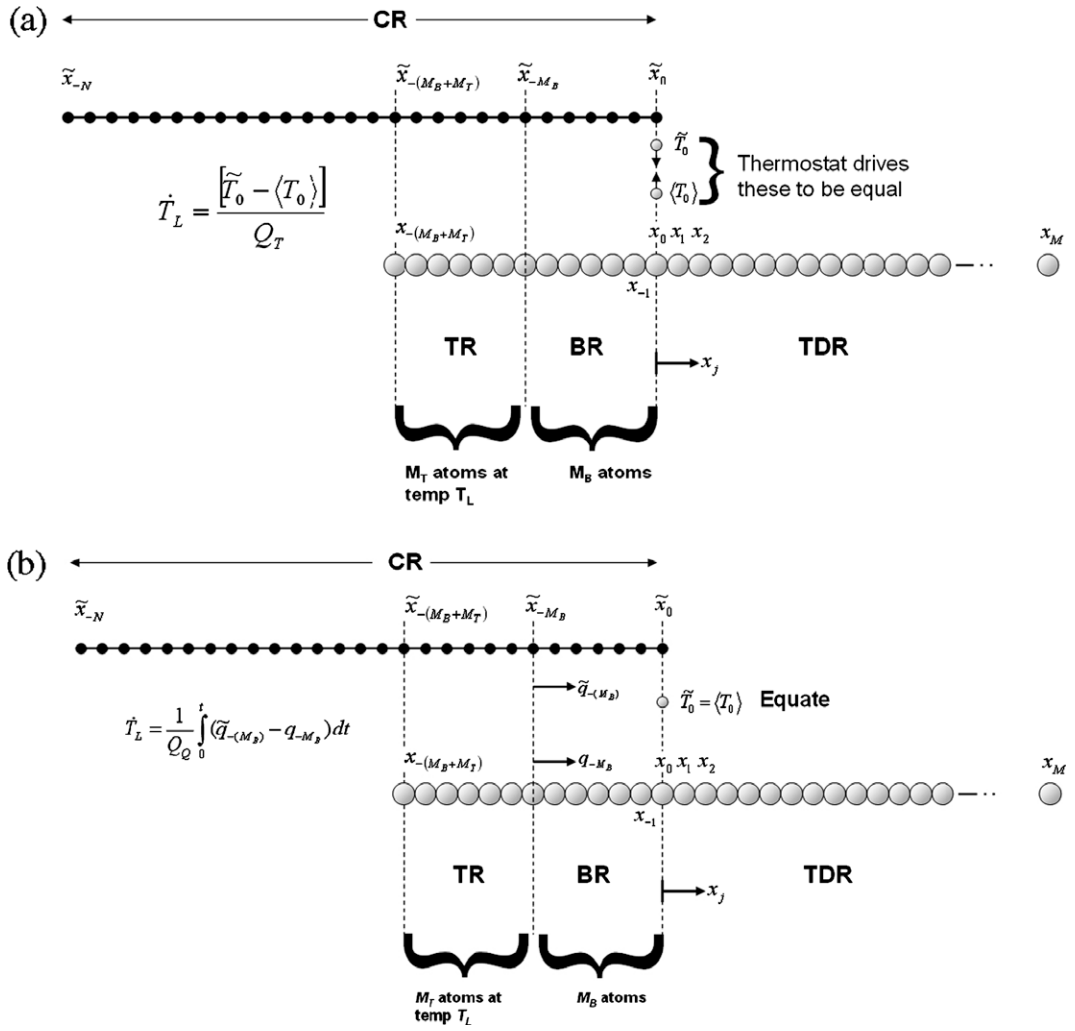


**Fig. 4.** A schematic diagram of the coupling between the NEMD simulation and the finite difference continuum representation for (a) steady state and (b) transient thermal boundary conditions. This is only shown for the left hand end of the rod, as a similar situation exists at the other end. The steady state boundary condition drives the atomistic and continuum temperatures at the CR/TDR interface to the same value using (2.9) and (3.6). The transient boundary condition is slightly more expensive to calculate as it conserves the heat fluxes across the TR/BR interface. This interface is chosen (rather than the BR/TDR interface) to minimize delays in the responsiveness of the thermostat. The transient boundary condition is also applicable to steady state conditions.

is readily determined to be $c = \frac{d(3k_BT)}{dT} = 3k_B$. The Debye model predicts the heat capacity for the more general case [30] although this quantum phonon effect is not captured by classical molecular dynamics.

To implement a compatible continuum model it is necessary to have knowledge of the relevant macroscopic material parameters. In this case the only unknown parameter is the thermal conductivity. Close inspection of the steady state temperature profiles within the TDR in Fig. 3 show that it is not precisely linear due to the variation in the thermal conductivity with temperature. To first order, it is proposed that the conductivity is a linear function of temperature such that $k(T) = k_0 + \nabla k T$. In the steady state the heat flux of (2.1) has a constant value

$$q_{ss} = k(T)\frac{dT}{dx}. \tag{3.3}$$

This is readily integrated to give

$$q_{ss}x = k_0(T - T_0) + 1/2\nabla k(T^2 - T_0^2) \tag{3.4}$$

where the position is $x = 0$ at the $j = 0$ slice at which $T = T_0$. The quadratic of (3.4) closely fits the observed temperature distributions shown in Fig. 3, but knowledge of the steady state heat flux $q_{ss}$ is required to determine an absolute thermal conductivity value.

The instantaneous (spatially averaged) atomistic heat flux between each slice, $q_j$, at time $t$ can be determined from

$$q_j(t) = q_{j-1}(t) + \sum_{\text{slice}\,j} \mathbf{f}_T \cdot \dot{\mathbf{x}} + \frac{1}{2\tau}\sum_{\text{slice}\,j} m\left[|\dot{\mathbf{x}}(t)|^2 - |\dot{\mathbf{x}}(t-\tau)|^2\right] \tag{3.5}$$

where the first term on the right hand side, $q_{j-1}$, is the heat flow out of the previous slice, the second term is the rate at which the thermostat adds energy to slice $j$ (zero in BR and TDR) and the third term is the rate of change in the kinetic energy of the slice over the time step $\tau$. The force on each atom due to the thermostat is $\mathbf{f}_T = R\mathbf{f} - \gamma m\dot{\mathbf{x}}$ from (2.4) for the stochastic thermostats and $\mathbf{f}_T = -\xi m\dot{\mathbf{x}}$ from (2.5) for the Nosé–Hoover thermostat. The heat flux into the first slice (in the TR) at $j = -(M_B + M_T)$ is zero as these atoms are fixed in space. Hence the time-averaged heat flux $\langle q_j\rangle$ can be calculated for every slice using (3.5). This was done for the steady state simulations of Fig. 3. The heat flux in the TDR was found to be constant with $q_{ss} = \langle q_j\rangle$ for all $j - 0,\ldots,M$. Eq. (3.4) was then fitted to the temperature distribution and the thermal conductivity determined to be $k_0 = 1.016$ W/(m K) and $\nabla k = -0.02$ W/(m K). This calibration of the thermal conductivity from a single steady state NEMD simulation only needs to be conducted once for a given interatomic potential.

Note that the long boundaries of the rod are periodic so the non-uniform thermal expansion of the rod cannot be accommodated. The compressive strain in the rod therefore increases with the temperature and varies along its length. It is possible that the thermal conductivity has a significant dependence on the strain state [16]. Ideally a continuum model will not require material parameters to be pre-determined, especially if they are a complex function of state, e.g. temperature, strain and crystallographic orientation. It is often difficult or too time consuming to completely characterise a parameter in terms of the many state variables. Therefore it is preferable to determine these parameters on-the-fly [5] or at least refine them during the course of a simulation. This is discussed within the context of the coupling methodology proposed in the following sub-section.

### 3.2. Thermal boundary conditions for steady state coupled atomistic/continuum simulation

Two finite difference continuum regions (CR) containing $N + 1$ nodes and defined by (3.1) are now coupled to each of the two ends of the atomistic NEMD simulation, as shown in Fig. 4(a) (for the left hand region only). The nodal positions go from $\tilde{x}_{-N}$ to $\tilde{x}_0$ for the left hand CR and from $\tilde{x}_M$ to $\tilde{x}_{M+N}$ for the right hand CR. The nodes at $\tilde{x}_0$ and $\tilde{x}_M$ coincide with the edges of the TDR in the NEMD simulation at slices $j = 0$ and $j = M$. The only prescribed boundary conditions (temperatures) are now at the outermost boundaries of the finite difference grid and are denoted $\widetilde{T}_{-N}$ and $\widetilde{T}_{M+N}$. Unlike the analysis of Section 2.3, the target temperatures at the boundaries of the TDR, $T_0$ and $T_M$, are now no longer fixed at a particular value. The NEMD simulation is now only of interest in the TDR. The atomistic TRs and BRs are only used to control the thermal boundary conditions to the TDR. These boundary conditions are determined by matching conditions at the interface between the CR and TDR at $j = 0$ and $j = M$. For steady state analysis it is sufficient to simply specify that the desired temperatures for the edges of the TDR should be the same as those at the matching node in the finite difference model such that we defined $T_0$ and $T_M$ by

$$T_0 = \widetilde{T}_0, \quad T_M = \widetilde{T}_M \tag{3.6}$$

The thermostat temperatures are determined by the feedback control (2.9) as before, as shown in Fig. 4(a). Results are shown in Fig. 5 for the stadium damping thermostat for $N = 20$. The temperature gradient is maintained within the TDR, although this time the temperatures are defined at the remote boundaries of the finite difference simulation not at the edges of the TDR. The fixed end temperatures are taken to be $\widetilde{T}_L = \widetilde{T}_{-N} = 40$ K and $\widetilde{T}_R = \widetilde{T}_{M+N} = 20$ K. The temperature profiles in the CRs at the left and right hand sides and the temperature in the TDR are shown. The unphysical temperatures in the TRs and BRs are not shown in these or subsequent simulation results. It is found that the temperature profile quickly settles down to the expected stable steady state. This is a considerable achievement as the atomistic region is highly dynamic and the instantaneous temperature at the continuum/atomistic (CR/TDR) interface fluctuates rapidly. The stability of the method is not

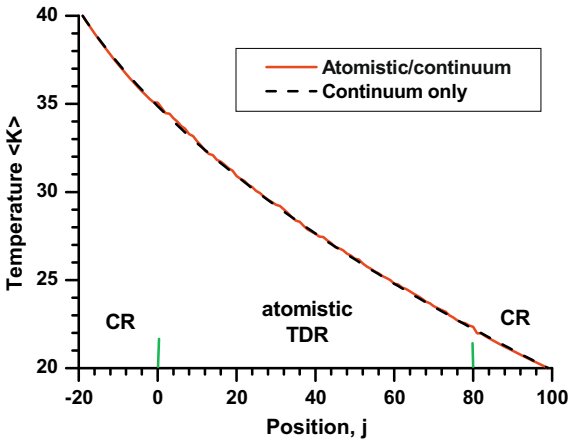


**Fig. 5.** Steady state results for the coupled atomistic-continuum simulation. Target temperatures of 40 K and 20 K are now prescribed at the edges of the continuum regions (at $j = -20$ and $j = 100$). The target temperatures at the boundaries of the TDR (at $j = 0$ and $j = 80$) are now variable and determined from the coupling between the continuum model and the NEMD simulation.

found to be very sensitive to the choice of the material parameters in the CR ($k_0, \nabla k$ and $c$) or those in the TR ($Q_T$) which is important. A discontinuity in the gradient of the temperature curves at this interface is only observed if there is a significant thermal conductivity mismatch between the CR and TDR. As the heat flux and temperature gradient are known at all points in the simulation it is a simple matter to determine the thermal conductivity during the simulation. This value can be used to refine the measured value on-the-fly. This is especially useful if the conductivity is expected to change significantly due to a variation in the state variables during the simulation.

### 3.3. Thermal boundary conditions for transient coupled atomistic/continuum simulation

The previous work in this paper has only considered the steady state response of NEMD simulations. However, one of the advantages of a continuum model is that full control of the remote boundary conditions is obtained. These boundary conditions are dependent on the temperature or the heat flux at the boundary and can therefore be functions of time. In this section the methodology is extended to consider such cases. The thermostat temperatures will evolve over time for transient problems. Therefore it is necessary to determine the rate of change of the target temperatures in the TRs. In addition, simply using the temperature matching condition (3.6) is not sufficient as time delays and thermal fluctuations will allow thermal energy to be lost over time. Therefore we explicitly enforce the conservation of thermal energy between the models. A first approach would be to simply equate the continuum and atomistic heat fluxes at the CR/TDR interface. For the left hand side shown in Fig. 4(b) this would require $\tilde{q}_0 = q_0$. However, the instantaneous atomistic heat flux is rapidly changing so this is only enforced on average over time. This is achieved by controlling the thermostat target temperatures at each end such that

$$\dot{T}_L = \frac{1}{Q_Q}\int_0^t (\tilde{q}_m - q_m)dt, \quad \dot{T}_R = \frac{1}{Q_Q}\int_0^t (q_n - \tilde{q}_n)dt \tag{3.7}$$

where $Q_Q$ determines the response rate of the system to disparities in the heat flux and the integers $m$ and n are the indices of the slices where this condition is to be applied. The right hand side of Eq. (3.7) is the difference between the total thermal energy that has left the continuum region and that which has entered the atomistic region (or vice versa). The time-ensemble average of this quantity should be zero (i.e. heat flux must be conserved). The left hand side shows that the thermostat temperatures evolve over time to achieve this. The integral ensures that no heat is lost over time. The temperatures in the atomistic and continuum regions do not need to be connected in this case, as long as the values at the CR/TDR interface are initially the same. Conservation of the heat flux through (3.7) should ensure that the atomistic and continuum descriptions of the temperature at the interface should remain the same thereafter. However, it is found to be of added benefit to equate the continuum temperature at the CR/TDR interface to the atomistic value such that

$$\widetilde{T}_0 = \langle T_0 \rangle, \quad \widetilde{T}_M = \langle T_M \rangle \tag{3.8}$$

to give additional feedback to the algorithm and reduce its sensitivity to parameter selection. Note that this is different to the steady state temperature matching condition (3.6). In that case, the MD target boundary temperature was specified to be the continuum temperature value at that point. In (3.8) the temperature in the continuum is taken to be the ensemble-averaged temperature at the equivalent point in the MD simulation. The remaining issue when dealing with thermal transients is the responsiveness of the system. There is an inherent time delay in the system as a change in the target temperature of the TR takes a small time to effect a change in the heat flux at another point in the simulation. This is unavoidable with this

methodology so the objective is to minimize the effect of this delay. This can be achieved by optimizing the position, $m$, at which heat flux conservation between the continuum and atomistic models is enforced. Selecting this to be the BR/TDR interface ($m = 0$ and $n = M$) gives reasonable results although there is still a small noticeable delay between the two descriptions. It is found that the optimal position is at the TR/BR interface as shown in Fig. 4(b). This minimizes the distance between the thermostat and the system controller (3.7). The BR has been reduced in size to $M_B = 5$ based on the steady state observations for the stadium damping thermostat in Fig. 3. This is because the system is more responsive if the buffer zone is smaller.

Results are shown in Fig. 6 for four different test cases. These demonstrate the ability of the model to respond to changes in the boundary conditions at the atomistic/continuum interface over time, including multiple reversals in the heat flux from heat entering to heat leaving the boundary. Even though the thermal change is large and rapid, there is no observable delay between the response of the continuum and atomistic regions. In each case the combined atomistic/continuum results agree very well with the results from a full finite difference simulation (shown as dashed lines). All parameters remain the same as before with the additional parameter $Q_Q = 6\varepsilon\tau$. The choice of value for this parameter is not critical and the algorithm is not particularly sensitive to it. All the graphs are plots of the average of multiple simulations at $10{,}000\tau$ intervals to reduce the effect of thermal noise on the image.

The first case shown in Fig. 6(a) has the remote boundary temperatures fixed at $\widetilde{T}_L = 40$ K and $\widetilde{T}_R = 20$ K. The simulation starts with one half held at 40 K while the other half is held at 20 K. The centre slice is initially fixed such that no heat flows between the two halves while the system is thermalised. After sufficient time the centre slice is allowed to interact as normal, and the system evolves towards a steady state. The second case is shown in Fig. 6(b). Here, the system is allowed to

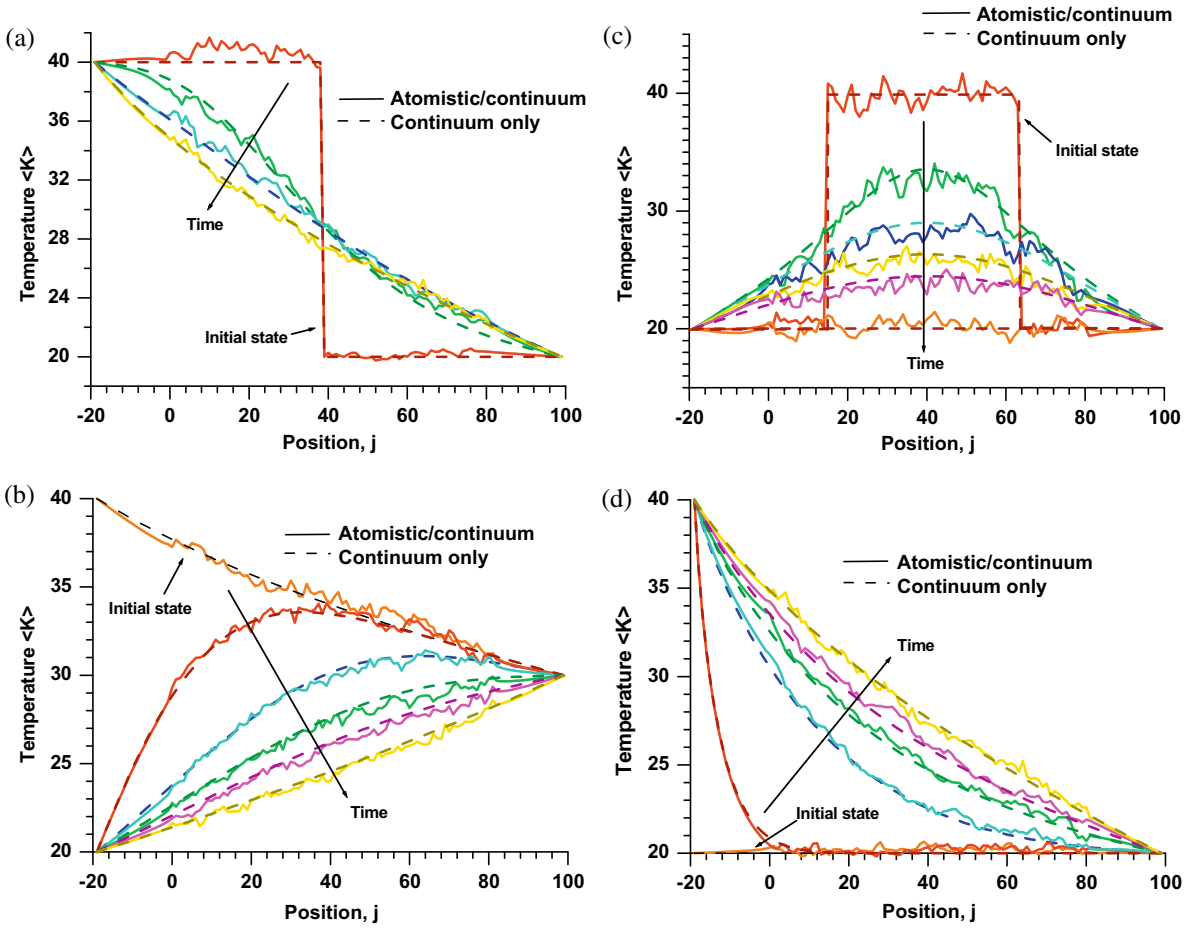


**Fig. 6.** Snapshots of the temperature profile evolution for transient boundary conditions for an entirely continuum model (dashed lines) and a coupled atomistic/continuum model, where the TDR is $0 \leqslant < j \leqslant 80$. Four cases are considered: (a) the simulation starts with one half held at 40 K while the other half is held at 20 K; (b) the system is allowed to reach a steady state with the outer edges set at 40 K and 30 K. Then the left outer edge is suddenly dropped to 20 K and the system allowed to evolve towards its new steady state; (c) a central region within the TDR is thermalised at 40 K while all surrounding atoms and the continuum are at 20 K. The hot inner region cools over time until the system has cooled down entirely to a steady state temperature of 20 K after a long-time; and (d) initially at 20 K, the left hand boundary is subject to an instantaneous temperature increase to 40 K. Again, the system evolves as expected towards the steady state. In each case the coupled simulation result agrees very well with the result from the continuum simulation.

reach a steady state with the outer continuum temperatures set at $\widetilde{T}_L = 40$ K and $\widetilde{T}_R = 30$ K. The left outer edge $\widetilde{T}_L$ is then instantaneously dropped to 20 K, and the system allowed to evolve. The boundary conditions at the CR/TDR interface are truly transient as the temperature and heat flux evolves continuously over time at this point. The third case is shown in Fig. 6(c). A central part of the TDR is thermalised at 40 K while all surrounding atoms and the CRs are thermalised at 20 K. As in Fig. 6(a), this initial distribution is achieved by temporarily fixing the atoms between these different temperature zones. When the interactions are turned on again, the 40 K region rapidly cools down to the temperature of the surrounding 20 K region, reaching equilibrium after a time of $10^5\tau$. The fourth case, shown in Fig. 6(d), is for a coupled system that is initially thermalised at 20 K. The left hand temperature $\widetilde{T}_L$ is then instantaneously increased to 40 K. The system evolves as expected towards the steady state. As expected the transient boundary conditions produce the same result as the steady state boundary conditions once equilibrium has been achieved. However, the steady state boundary conditions in subsection 3.2 are still of value for purely steady state problems as they do not require the additional complication of the flux calculation of (3.5). Importantly, the continuum coupling has virtually no computational overhead, with the NEMD part of the simulation accounting for practically all the processor time. Rapid sinusoidal variation of the external boundary conditions has also been investigated with excellent correspondence between the purely continuum and the hybrid models even after many hundreds of cycles.

In the problems of Fig. 6, the system always evolves towards a steady state. A situation which better demonstrates the potential of the coupled atomistic/continuum method proposed here is shown in Fig. 7. This is a situation where the system is large (effectively infinite) and will not reach a steady state (within a finite time). Energy is constantly injected into the central slice of the TDR by adding a random force to the atoms there. The temperature of these atoms increases and heat flows out towards the boundaries. Fig. 7 shows the temperature profile evolution for two approximations to the full atomistic simulation of this problem (where we imagine that it is not possible to obtain the full solution due to computational limitations). Case (A) is an atomistic approximation of a reduced system employing a 100 slice NEMD simulation with the temperature fixed at 20 K at the local boundaries (using the algorithm in Section 2.3); case (B) represents a similar NEMD simulation of 100 slices coupled to a large continuum region. This is expected to provide more realistic boundary conditions as the temperature at the atomistic/continuum boundaries can evolve over time. The inset in Fig. 7 shows the temperature profile at a time $t = 10^4\tau$ when heat is just beginning to cross the atomistic system boundaries. At this point the profiles are similar. The main figure illustrates the thermal profile at a much later time, $t = 10^5\tau$ (the earlier case (B) $t = 10^4\tau$ result is shown again for reference). The temperature profiles are now quite different. The constraint of the local fixed temperature boundary conditions in case (A) has had a major effect. A steady state temperature gradient has developed such that the heat flow from the centre balances the rate of energy input into the system. This is an artefact of the system size. In case (B) the atomistic simulation is embedded within a large continuum region so that it cannot see the remote boundaries within the time scale of the simulation. It is important to note that case (B) does not require significantly greater computational time that case (A), i.e. the continuum region and coupling algorithm has a very small computational overhead compared to the NEMD simulation. This class of problem is representative of a situation where work is being done on an atomistic simulation but the simulation is reduced in size (for computational efficiency) such that heat is crossing the simulation boundaries (without being properly accounted for) during the simulation time, e.g. differential thermal contact such as an AFM tip on a substrate [21], nanoindentation [14,15], wear [12] or crack growth [31].

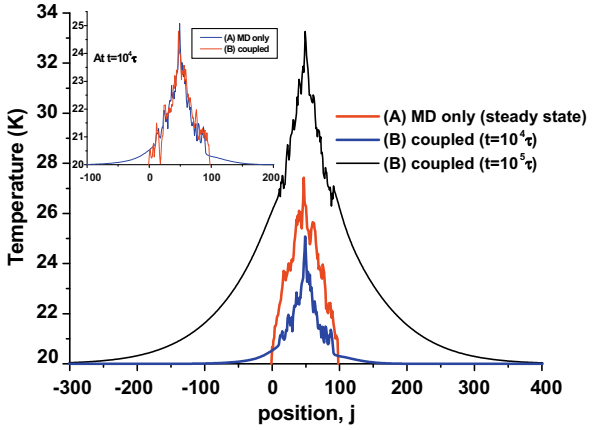


**Fig. 7.** Transient analysis for two identical NEMD simulations except for their boundary conditions: case (A) has the temperature fixed at 20 K at its boundaries (at $j = 0$ and $j = 100$) whilst the other, case (B), has its boundaries coupled to a much larger continuum simulation. Energy is injected into the centre of the NEMD simulation at $j = 50$ causing the temperature at the centre to increase and heat to flow out towards the boundaries. The inset picture compares cases (A) and (B) at a time ($t = 10^4\tau$) when the heat flux is starting to be affected by the boundary conditions. At this point the temperature profiles are similar. As the system continues to evolve, the temperature gradient in case (A) balances the rate of energy input into the system and achieves a steady state. This is a direct consequence of the local boundary conditions. Meanwhile, case (B) continues to evolve as heat flows across the atomistic/continuum boundary into the large CR which provides more appropriate boundary conditions.

## 4. Discussion and conclusions

A simple molecular dynamics/continuum coupling algorithm for heat transfer in solids has been developed which does not depend upon the underlying interatomic potential model employed. This should therefore be useful in a wide range of areas in the modelling of solid crystals [32–35]. The models in this paper have been developed within the context of a quasi one-dimensional problem in which net heat flow only occurs in one direction. The situation is slightly more complicated for controlling the temperature in more than one direction but the method is still applicable. The thermostatting region will no longer necessarily drive the boundary of the TDR towards a uniform temperature, i.e the temperature can vary around the boundary. In the case of local thermostats such as Langevin and stadium damping this is not a problem as each atom can be driven towards a different temperature. Li and Weinan [5] have shown that global thermostats such as Nosé–Hoover can also achieve this by dividing the thermostatted region in to sections along the periphery and having a different target temperature in each. However, this sectioning can complicate the algorithm and leads to an increase in the number of thermostatting variables $\xi$. This is not the case for the local thermostats, where atoms can be individually labelled as thermostatted or unthermostatted. Hence the TR can be easily changed to accommodate an expansion/contraction of the TDR over time by altering which atoms are considered to be part of it. The steady state boundary conditions considered in Sections 2.3 and 3.2 require a relationship between the target temperatures on the BR/TDR boundary and the thermostat temperatures with the TR, similar to that given in (2.9). This is obvious if a boundary has a uniform temperature (as considered here) but more complicated if the temperature varies continuously along the boundary, where a particular thermostatted atom will affect the temperature of a number of target temperature atoms and vice versa. In this case the thermostat temperatures can be related to the target temperatures through a compact local proximity weighting kernel. The more general transient boundary conditions considered in Section 3.3 however only require a knowledge of the heat flux which can be readily calculated without additional complications to the algorithm.

The issue of thermal expansion has been briefly mentioned in Section 3.1. Coupled thermoelastic boundary conditions need to be considered to correctly model this phenomenon. Qu et al. [10] have proposed an isothermal model for coupled continuum/atomistic elasticity problems using a stadium damping thermostat at the boundary to avoid adverse phonon reflection. This method is compatible with the approach here for combined coupled atomistic/continuum thermoelastic problems. This would be a beneficial extension, as stresses due to thermal expansion will always be an issue in complete NEMD simulations. The quasi-elastostatic continuum far-field is coupled to the quasi-static atoms at the outer edge of the TDR. The force on the nodes of the finite element field must balance the time-ensemble average force on their equivalent atoms in the TDR. The only significant difference between the thermal equilibrium case [5] and the non-equilibrium case considered here is that the additional TR and BR need to be introduced to control the thermal boundary conditions of the TDR. Away from equilibrium the temperatures in the TR are unphysical and chosen to achieve the desired target temperatures at the TDR boundary. This leads to unphysical thermal expansion or contraction of the TR and BR which would affect the stress state within the TDR. To implement the method of Qu et al. [10] it would be necessary to find some way of enforcing the thermal expansion to be that associated with the physical temperature at the same point in the finite element field. This could be achieved through a stadium version of the Langevin barostat to also regulate the hydrostatic pressure of each atom [36].

In summary, a method for controlling the thermal boundary conditions of non-equilibrium molecular dynamics (NEMD) simulations has been presented in Section 2. The method is simple to implement into a conventional molecular dynamics code and independent of the atomistic model employed. The crystal is thermostatted at the boundaries to control the temperature at the edges of the true dynamics region (TDR). A small buffer region lies between these two regions to avoid the TDR being corrupted by boundary effects. This simple feedback control has been shown to work for a quasi one-dimensional example of heat flow down a three-dimensional rod of uniform cross-section. These boundary conditions are of use for analysing the heat transfer across nanoscale features [37] such as grain boundaries [24], nanowires [23,38,39] and nanoconstrictions [21]. As the model does not rely on the potential, there is a possibility that the potentials could be altered to incorporate quantum effects [40]. The method for controlling the boundary conditions of NEMD simulations has been extended in Section 3 to allow atomistic/continuum models to be thermally coupled concurrently for the analysis of steady state and transient heat conduction problems. The effectiveness of this algorithm has been demonstrated through a number of examples.

## Acknowledgments

KJ gratefully acknowledges the support of EPSRC Grant No. EP/P501547/1. SG is grateful for the award of a Royal Academy of Engineering-Leverhulme Trust Senior Research Fellowship 2007–2008 for supporting this research.

## References

[1] J.Q. Broughton, F.F. Abrahams, N. Bernstein, E. Kaxiras, Concurrent coupling of length scales: methodology and application, Phys. Rev. B 60 (1999) 2391.
[2] W.A. Curtin, R.E. Miller, Atomistic/continuum coupling in computational materials science, Modell. Simul. Mater. Sci. Eng. 11 (2003) R33–R68.
[3] S.P.A. Gill, Z. Jia, B. Leimkuhler, A.C.F. Cocks, Rapid thermal equilibration in coarse-grained molecular dynamics, Phys. Rev. B 73 (2006) 184304.
[4] X. Li, W.E. Weinan, Variational boundary conditions for molecular dynamics simulations of solids at low temperature, Commun. Comp. Phys. 1 (2006) 135–175.
[5] X. Li, W.E. Weinan, Multiscale modelling of the dynamics of solids at finite temperature, J. Mech. Phys. Solids 53 (2005) 1650–1685.

[6] W.K. Liu, E.G. Karpov, S. Zhang, H.S. Park, An introduction to computational nanomechanics and materials, Comput. Meth. Appl. Mech. Eng. 193 (2004) 1529.
[7] W.K. Liu, H.S. Park, D. Qian, E.G. Karpov, H. Kadowaki, G.J. Wagner, Bridging scale methods for nanomechanics and materials, Comput. Meth. Appl. Mech. Eng. 195 (2006) 1407–1421.
[8] H.S. Park, W.K. Liu, An introduction and tutorial on multiple-scale analysis in solids, Comput. Meth. Appl. Mech. Eng. 193 (2004) 1733–1772.
[9] H.S. Park, E.G. Karpov, W.K. Liu, A temperature equation for coupled atomistic/continuum simulations, Comput. Meth. Appl. Mech. Eng. 193 (2004) 1713–1732.
[10] S. Qu, V. Shastry, W.A. Curtin, R.E. Miller, A finite temperature dynamic coupled atomistic/discrete dislocation method, Modell. Simul. Mater. Sci. 13 (2005) 1101.
[11] R.E. Rudd, J.Q. Broughton, Concurrent coupling of length scales in solid state systems, Phys. State Solid B217 (2000) 5893.
[12] L.E. Shilkrot, R.E. Miller, W.A. Curtin, Multiscale plasticity modelling: coupled atomistic and discrete dislocation mechanics, J. Mech. Phys. Solids 52 (2004) 755–787.
[13] S.P. Xiao, T. Belytschko, A bridging domain method for coupling continua with molecular dynamics, Comput. Meth. Appl. Mech. Eng. 193 (2004) 1645–1669.
[14] W.K. Liu, E.G. Karpov, H.S. Park, Personal communication.
[15] L.M. Dupuy, E.B. Tadmor, R.E. Miller, R. Phillips, Finite-temperature quasicontinuum: molecular dynamics without all the atoms, Phys. Rev. Lett. 95 (2005) 060202.
[16] S. Bhowmick, V.B. Shenoy, Effect of strain on the thermal conductivity of solids, J. Chem. Phys. 125 (2006) 164513.
[17] P. Heino, Thermal conductivity and temperature in solid argon by non-equilibrium molecular dynamics simulations, Phys. Rev. B 71 (2005) 144302.
[18] Z. Huang, Z. Tang, Evaluation of momentum conservation influence in non-equilibrium molecular dynamics methods to compute thermal conductivity, Physica B 373 (2006) 291–296.
[19] S. Lepri, R. Livi, A. Politi, Energy transport in anharmonic lattices close to and far from equilibrium, Physica D 119 (1998) 140–147.
[20] S. Lepri, R. Livi, A. Politi, Thermal conduction in classical low-dimensional lattices, Phys. Rep. 377 (2003) 1.
[21] R. Prasher, Diffraction limited phonon thermal conductance of nanoconstrictions, Appl. Phys. Lett. 91 (2007) 143119.
[22] P.K. Schelling, S.R. Phillpot, P. Keblinski, Comparison of atomic-level simulation methods for computing thermal conductivity, Phys. Rev. B 65 (2002) 144306.
[23] D. Segal, A. Nitzan, Thermal conductance through molecular wires, J. Chem. Phys. 119 (13) (2003) 6840.
[24] T. Watanabe, B. Ni, S.R. Phillpot, Thermal conductance across grain boundaries in diamond from molecular dynamics simulation, J. Appl. Phys. 102 (2007) 063503.
[25] T. Terao, F. Muller-Plathe, A non-equilibrium molecular dynamics method for thermal conductivities based on thermal noise, J. Chem. Phys. 122 (2005) 081103.
[26] A. Rahman, Correlations in the motion of atoms in liquid argon, Phys. Rev. 136 (2A) (1964).
[27] L. Verlet, Computer ‘‘experiments” on classical fluids i thermodynamical properties of Lennard–Jones molecules, Phys. Rev. 159 (1) (1967) 98.
[28] K. Binder, J. Horbach, W. Kob, W. Paul, F. Varnik, Molecular dynamics simulation, J. Phys.: Condens. Matter 16 (2004) S429–S4543.
[29] W.M.G. Hoover, K. Aoki, C.G. Hoover, S.V. De Groot, Time-reversible deterministic thermostats, Physica D 187 (2004) 253–267.
[30] J.R. Hook, H.E. Hall, Solid State Physics, second ed., J. Wiley & Sons Ltd., 1991.
[31] B.L. Holian, R. Ravelo, Fracture simulations using large-scale molecular-dynamics, Phys. Rev. B. 51 (1995) 11275–11288.
[32] W. Ren, Analytical and numerical study of coupled atomistic-continuum methods for fluids, J. Comp. Phys. 227 (2007) 1353–1371.
[33] J. Liu, S. Chen, X. Nie, M.O. Robbins, A continuum-atomistic simulation of heat transfer in micro-and nano-flows, J. Comp. Phys. 227 (2007) 279–291.
[34] E.G. Flekkoy, R. Delgado-Buscalioni, P.V. Coveney, Flux boundary conditions in particle simulations, Phys. Rev. B 72 (2005) 026703.
[35] T. Werder, J.H. Walther, P. Koumoutsakos, Hybrid atomistic-continuum method for the simulation of dense fluid flows, J. Comp. Phys. 205 (2005) 373–390.
[36] D. Quigley, M. Probert, Langevin dynamics in constant pressure extended systems, J. Chem. Phys. 120 (2004) 11432.
[37] G. Chen, D. Borca-Tasciuc, R.G. Yang, Nanoscale Heat Transfer, Encyclopedia of Nanoscience and Nanotechnology, American Scientific Publishers, 2004.
[38] W. Huang, G. Huang, L. Wang, B. Huang, Phonon-cavity-enhanced low temperature thermal conductance of a semiconductor nanowire with narrow constrictions, Phys. Rev. B 75 (2007) 233415.
[39] W. Tian, R. Yang, Effect of interface scattering on phonon thermal conductivity percolation in random nanowire composites, Appl. Phys. Lett. 90 (2007) 263105.
[40] J. Wang, Quantum thermal transport from classical molecular dynamics, Phys. Rev. Lett. 99 (2007) 160601.